Journal of Materials Chemistry A

Accepted Manuscript

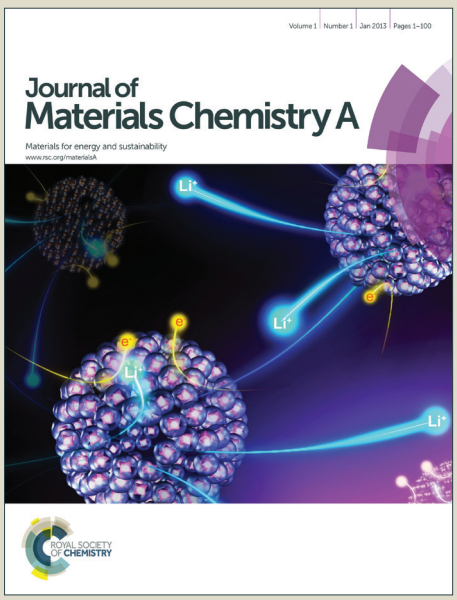

ROYAL SOCIETY OF CHEMISTRY

www.rsc.org/materialsA

Journal of Materials Chemistry A

Dynamic Article Links ►

Cite this: DOI: 10.1039/c0xx00000x

Paper

www.rsc.org/xxxxxx

High-energy, full concentration-gradient cathode material with excellent cycle and thermal stability for lithium ion batteries

P. Y. Hou,[a] L. Q. Zhang,*[b] and X. P. Gao*[a]

Received (in XXX, XXX) Xth XXXXXXXXX 20XX, Accepted Xth XXXXXXXXX 20XX

DOI: 10.1039/b000000x

Ni-rich $Li[Ni_{1-x}M_x]O_2$ (M =Co, Mn and Al) cathodes have shortcomings of poor thermal stability at the delithiated state and insufficient cycle performance, which are unsatisfied for commercial application in lithium ion batteries. Herein, a nickel-rich lithium transition-metal oxide with the full concentration-gradient structure is designed to overcome those problems. In the full concentration-gradient oxide, the nickel concentration decreases linearly, and the manganese concentration increases gradually, whereas cobalt concentration remains constant from the center to surface of each particle based on the energy disperse spectrum (EDS) analysis on cross-section of a single particle. Firstly, the full concentration-gradient precursor is successfully prepared via a newly developed co-precipitation route. After lithiation at 800 °C, the as-prepared full concentration-gradient and normal oxides could be indexed to a typical layered structure with an $R\bar{3}m$ space group as detected by X-ray diffraction (XRD). Correspondingly, the full concentration-gradient layered oxide delivers more excellent cycle stability (especially at 55 °C), and thermal stability as compared with the normal layered oxide. It is also found that the Ni dissolution in electrolyte is more serious, resulting in inferior cycle life for the normal layered oxide. Whereas, the outer layer of the full concentration-gradient oxide is much more stable, contributing to such excellent cycle and thermal stability.

Introduction

Recently, more efforts have been focused on developing advanced lithium-ion batteries for hybrid electric vehicles (HEVs) and plug-in hybrid vehicles (PHEVs) due to global environmental concerns.[1] The desired cathodes with high energy density and good thermal stability play an important role in the development of next generation of Li-ion batteries. In particular, Ni-rich $Li[Ni_{1-x}M_x]O_2$ (M =Co, Mn, and Al) have attracted much attention as cathode materials for lithium ion batteries because of their low cost and high capacity.[2-6] Specifically, large reversible capacity about 200 mAh g^{-1} could be achieved via selecting appropriate amounts of Ni and other transition metal elements in Ni-rich $Li[Ni_{1-x}M_x]O_2$.[4,6-9]

Among those potential materials, $LiNi_{0.6}Co_{0.2}Mn_{0.2}O_2$ is investigated as one of the most promising materials for its easy synthesis and excellent high-rate performance in contrast with other higher Ni-rich oxide cathode materials.[6-12] However, Ni-rich oxide cathode materials show poor thermal stability due to the oxygen release from surface at the delithiated state, which can then react with the organic electrolyte and graphite anode to induce severe safety problems.[13-15] In addition, the high concentration of unstable Ni^{4+} occurs at the delithiated state, leading to high interfacial impedance and poor electrochemical performances due to the generation of NiO phase at the cathode surface.[16-18] Therefore, the cathode based on $LiNi_{0.6}Co_{0.2}Mn_{0.2}O_2$ oxide is structurally unstable during cycling, which may induce thermal runaway reactions on cathode. Therefore, various efforts are used to meet the challenge, including different synthesis methods,[10,19-20] and anion substitution.[12] Especially, it is found that core-shell or concentration-gradient structure could enhance the cycle ability and improve thermal stability of cathodes.[21-23] It is also noted that $Li[(Ni_{1/2}Mn_{1/2})_{1-x}Co_x]O_2$ (x = 0-1/3) oxides with high manganese content are commonly used as a shell or outer layer due to excellent cycling performance, and thermal stability.[24-30] In this case, the average oxidation state of Mn is tetravalent, so that the electrochemically inactive tetravalent Mn provides significant structural stability, maintaining the hexagonal structure during cycling, even at the high cut-off potential of 4.6 V.[25,31-34]

In this work, $LiNi_{0.6}Co_{0.2}Mn_{0.2}O_2$ is designed to a full concentration-gradient (FCG) structure, which would have advantages of core-shell and concentration-gradient structure, to improve the cycle and thermal stability. Here, Ni-rich $LiNi_{0.8}Co_{0.2}O_2$ and $LiNi_{0.4}Co_{0.2}Mn_{0.4}O_2$ with high Mn content are selected as the inner and outer composition, respectively, to provide structural and thermal stability. The full concentration-gradient oxide is achieved from full concentration-gradient precursors, prepared by a newly developed co-precipitation method with continuously changing the Ni/Co/Mn ratio.[35] As expected, the full concentration-gradient oxide presents excellent

electrochemical performance during cycling and good thermal stability.

Experimental

Preparation and characterization

Fig. 1 displays schematic diagram of the continuously stirred tank reactor (CSTR) in preparing the full concentration-gradient hydroxide precursors. To synthesize the full concentration-gradient precursor particles, stoichiometric $NiSO_4 \cdot 6H_2O$ and $CoSO_4 \cdot 7H_2O$ (cationic ratio of Ni:Co=8:2) were dissolved with a concentration of 2.0 mol L^{-1} as the starting materials (1 L) in Tank 2. During the reaction, Ni-rich solution was fed to the CSTR at a rate of 0.8 L h^{-1}. At the beginning of the reaction, 1 L, 2.0 mol L^{-1} manganese-rich aqueous solution (Tank 1, Ni/Co/Mn, 4:2:4 molar ratio) was continuously pumped into the stock solution Tank 2 containing the starting nickel-rich solution at a rate of 0.4 L h^{-1}. The mixed solution was continuously fed into a tank reactor. Both solutions in Tank 1 and Tank 2 are transferred completely at the same time by adjusting pumping rate of nickel-rich and manganese-rich solution. Then, the starting Ni-rich aqueous solution in Tank 1 was pumped into the CSTR (capacity of 10 L) at a rate of 0.8 L h^{-1} under a nitrogen atmosphere and precipitated with NaOH solution (10 mol L^{-1}) as the pH control agent and NH_4OH solution (2 mol L^{-1}) as the chelating agent in the CSTR under the constant pH (11.6). The temperature in the CSTR was kept constant at 50 °C, and mixing was achieved inside the CSTR by an impeller with a rate of 800 rpm. After 25 h, both solutions in Tank 1 and Tank 2 were completely consumed at the same time, leading to the full concentration-gradient precursors. The normal $[Ni_{0.6}Co_{0.2}Mn_{0.2}](OH)_2$ was also prepared via a similar co-precipitation route. Both precursor powders were obtained through filtering, washing, and drying overnight at 100 °C. Then, the prepared precursor powders were calcined with LiOH (molar ratio, Li/(Ni+Co+Mn)=1.05) at 800 °C for 16 h in air to form spherical lithiated layered powders.

X-ray Diffractometry (XRD, Rigaku D/MAX-2500) was used to characterize structure of the prepared materials. The morphology was observed by a scanning electron microscope (SEM, Hitachi S-4800). Energy dispersive X-ray spectroscopy (EDS, Hiroba EDX) was used to analyze the chemical composition of precursors and lithiated materials. The total chemical compositions of precursors and concentration of Ni, Co and Mn elements in electrolyte after different cycles at 55 °C were analyzed by an inductively coupled plasmas spectrometer (ICP, SPS 7800, Seiko Instruments).

Electrochemical measurement

To fabricate the working electrodes, the prepared materials were mixed with acetylene black and PVDF (83:10:7 in weight) in NMP. The obtained slurry was coated onto Al foil and dried at 80 °C for a day, followed by a roll-pressing. Prior to use, the working electrodes were dried again at 120 °C for half a day in a vacuum oven. The working electrodes were electrochemically characterized using a 2032 type of coin cell with lithium foil as the anode and 1 M $LiPF_6$ in ethylene carbonate diethyl carbonate (1:1 in volume) as electrolyte. The cells were preliminarily charged and discharged in the potential range of 3.0-4.4 V (vs.Li/Li^+) at 25 °C and 55 °C at 20 mA g^{-1} for initial three cycles, and measured at 100 mA g^{-1} for subsequent cycles with a LAND CT-2001A instrument (Wuhan). Electrochemical impedance spectra (EIS) were measured using a electrochemical workstation (Zahner IM6ex) in the frequency range of 100 kHz to 10 mHz. The cyclic voltammetry (CV) measurement was conducted with a electrochemical workstation (CHI 600A) at a scan rate of 0.1 mV s^{-1}. For differential scanning calorimetry (DSC) experiments, cells were initially charged to 4.4 V and disassembled carefully in the Ar-filled dry box. After disassembling the cells, the cathode materials were recovered from the current collector. The DSC data were collected in a differential scanning calorimeter (NETZSCH 204F1) using a temperature scan rate of 5 °C min^{-1} in the temperature range of 50-350 °C.

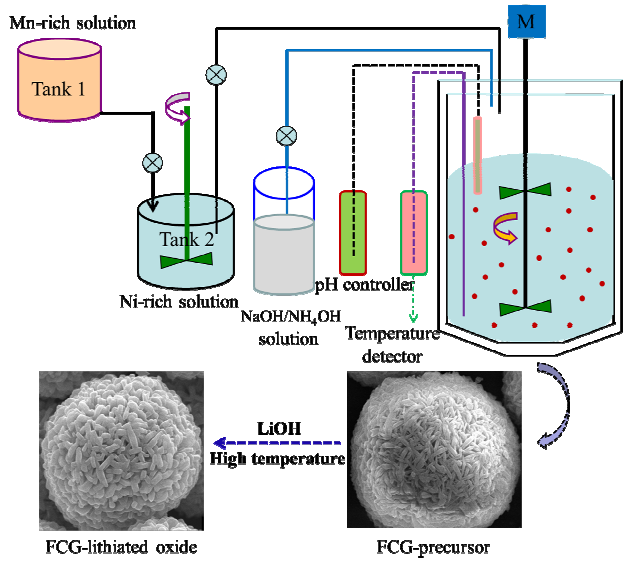

Fig. 1 Schematic diagram of the CSTR in preparing the full concentration-gradient hydroxide precursors and lithiated oxides; Tank 1: Ni/Co/Mn=4/2/4, Tank 2: Ni/Co=8/2.

Results and discussion

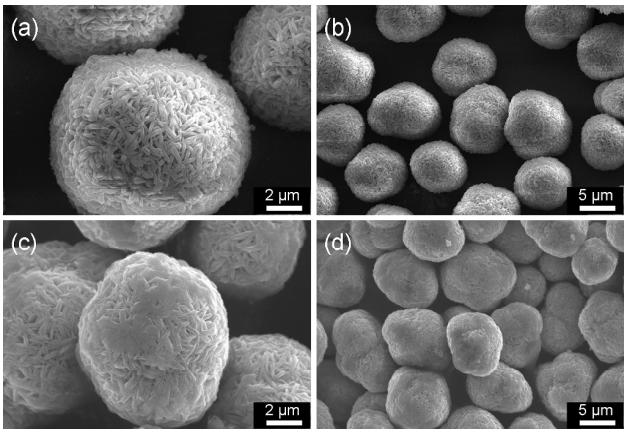

Fig. 2 SEM images (a) high- and (b) low-magnification of full concentration-gradient precursors, (c) high- and (d) low-magnification of normal precursors.

Fig. 2 shows SEM images of the precursors prepared by co-precipitation method. It is obvious that both full concentration-gradient and normal precursors show homogeneous spherical or ellipsoidal morphology, assembled with the needle-shaped

primary particles. The average chemical composition of full concentration-gradient and normal precursors are $[Ni_{0.605}Co_{0.197}Mn_{0.198}](OH)_2$ and $[Ni_{0.606}Co_{0.198}Mn_{0.196}](OH)_2$, respectively, as measured by ICP, in good consistent with the desired design.

To determine the compositional change in the full concentration-gradient structure, EDS is used to detect the composition on the cross-section of a single precursor particle, as displayed in Fig. 3. The concentrations of Ni, Co and Mn are plotted as a function of distance from the core center to the particle surface. Obviously, the Ni concentration decreases gradually from the center (about 78%) towards the outer layer of the particle, whereas the Mn concentration increases gradually from 2% (inner core) to 38% (surface). At the same time, Co remains constant in all full concentration-gradient structure. Therefore, the full concentration-gradient precursors are successfully achieved via a co-precipitation route, which are indispensable to prepare the full concentration-gradient oxide in the subsequent procedure. After lithiation, almost the same concentration change tendency is obtained for Ni, Mn and Co elements in the full concentration-gradient $LiNi_{0.6}Co_{0.2}Mn_{0.2}O_2$ oxide, as shown in Fig. 4. It means that the interdiffusion of Ni Co, and Mn cations can be ignored during lithiation at high calcination temperature, and the full concentration-gradient $LiNi_{0.6}Co_{0.2}Mn_{0.2}O_2$ oxide is obtained subsequently.

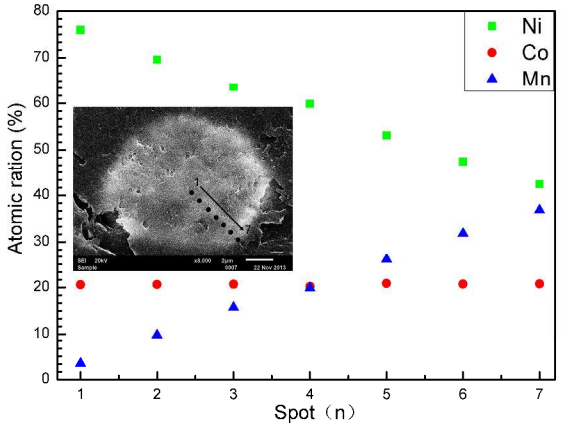

Fig. 3 EDS compositional change from the cross-section of a single full concentration-gradient precursor particle.

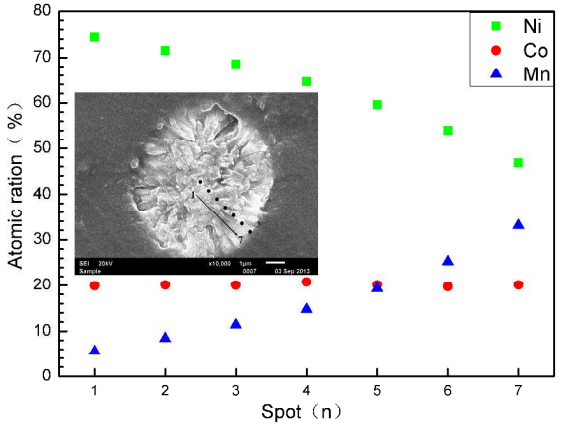

Fig. 4 EDS compositional change from the cross-section of a single full concentration-gradient oxide particle before cycling.

Fig. 5 shows XRD patterns of normal and full concentration-gradient $LiNi_{0.6}Co_{0.2}Mn_{0.2}O_2$ oxides calcined at 800 °C. Obviously, both oxides could be indexed to a well-defined hexagonal α-$NaFeO_2$-type structure with a space group of $R\bar{3}m$. Furthermore, the clear split between the adjacent peaks of (006)/(102) and (018)/(110) suggests a typical layered structure for both samples.[36] The lattice parameters of both oxides are calculated, as displayed in Table 1, indicating good similarity. When the calcination temperature is reduced, the resulting crystallinity of the final products is lower. Alternatively, high calcination temperature gives rise to severe diffusion of cations in the full concentration-gradient structure. Therefore, there is an optimum temperature to insure good crystallinity and low cation mixing within the full concentration-gradient oxide.

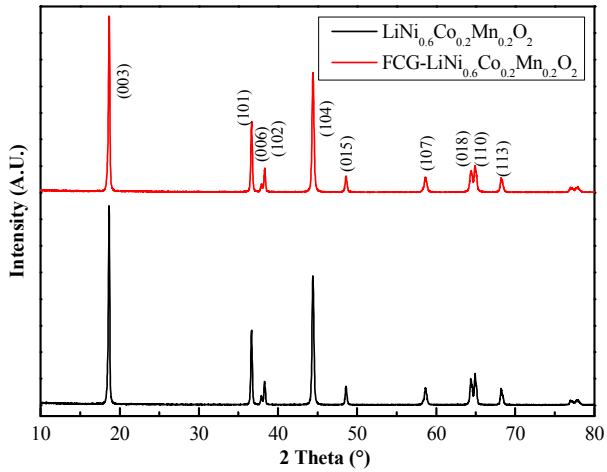

Fig. 5 XRD patterns of normal and full concentration-gradient (FCG) $LiNi_{0.6}Co_{0.2}Mn_{0.2}O_2$ oxides.

Table 1 Comparison of lattice parameters of full concentration-gradient and normal $LiNi_{0.6}Co_{0.2}Mn_{0.2}O_2$ oxides.

	a/Å	c/Å	Vol/Å
Full concentration-gradient oxide	2.8620	14.1854	100.63
Normal oxide	2.8624	14.1870	100.67

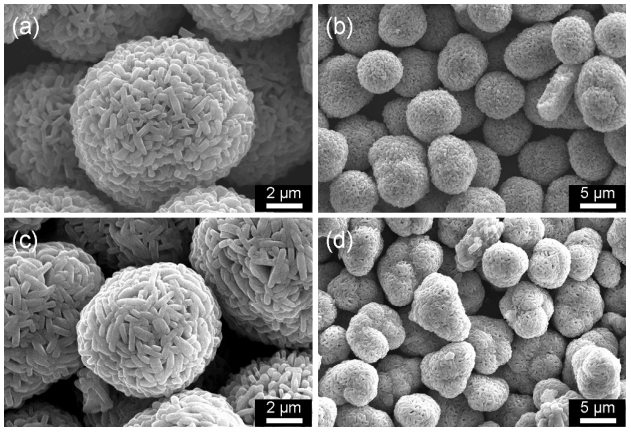

Fig. 6 SEM images of (a) high- and (b) low-magnification of full concentration-gradient oxide, (c) high- and (d) low-magnification of normal $LiNi_{0.6}Co_{0.2}Mn_{0.2}O_2$ oxide.

SEM images of the normal and full concentration-gradient oxides at high calcination temperature of 800 °C are shown in

Fig. 6. Clearly, the needle-shaped primary particles of precursors (as shown in Fig. 2) are transferred into platelike-shape after calcination at high temperature for both samples. Meanwhile, both oxide particles exist as spherical or ellipsoidal morphology, assembled with the platelike-shaped primary particles. It means that the morphology of particles and concentration of cations are almost identical for both oxides after lithiation at high temperature.

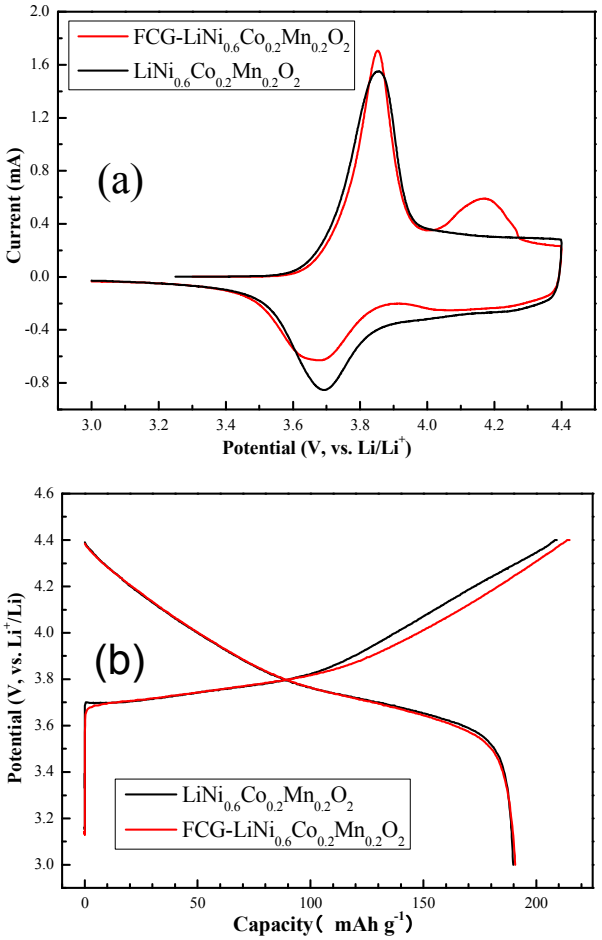

Fig. 7 Cyclic voltammograms (a) and initial charge-discharge curves (b) of the full concentration-gradient (FCG) and normal $LiNi_{0.6}Co_{0.2}Mn_{0.2}O_2$ oxides.

Fig. 7 illustrates cyclic voltammograms (CVs) of the normal and full concentration-gradient oxides at a scan rate of 0.1 mV s^{-1}, along with the initial charge–discharge curves between 3.0 and 4.4 V at the constant current density of 20 mA g^{-1} (0.1 C rate) and 25 °C. As shown in Fig. 7 (a), the sharp oxidation peak at 3.84 V (vs Li/Li^+) and low oxidation peak at 4.15 V (vs Li/Li^+) are found for the full concentration-gradient oxide in the initial anodic process due to multiphase transitions, which are attributed to the oxidation of Ni^{2+} to Ni^{4+} and Co^{3+} to Co^{4+}. Here, the appearance of the oxidation peak at 4.15 V (vs Li/Li^+) is the characteristics of Ni-rich oxides as cathodes, such as $LiNi_{0.8}Co_{0.2-x}Al_xO_2$,[37] $LiNi_{0.75}Co_{0.20}Mn_{0.05}O_2$,[38] and $LiNi_{0.8}Co_{0.1}Mn_{0.1}O_2$,[15] in agreement with the inner composition as shown in Fig 5. In the following cathodic process, the main peak at 3.71 V (vs Li/Li^+) is mainly related to the subsequent reduction of Co^{4+} to Co^{3+} and Ni^{3+} to Ni^{2+}. In addition, the weak peak at 4.05 V (vs Li/Li^+) is attributed to the reduction of Ni^{4+} to Ni^{3+}.[15,38] As shown in Fig. 7(b), the full concentration-gradient and normal $LiNi_{0.6}Co_{0.2}Mn_{0.2}O_2$ oxides deliver very high discharge capacity of 190.7 and 189.8 mAh g^{-1}, respectively. In particular, the potential polarization is lower for the full concentration-gradient oxide at high potential region (3.8-4.4 V).

As expected, full concentration gradient oxide presents good Li^+ intercalation stability in the potential range of 3.0 to 4.4 V at 25 °C and 55 °C, shown in Fig. 8 (a) and (c). At 25°C, the large capacity of 150.4 mAh g^{-1} and high energy density of 554.9 Wh Kg^{-1} are obtained for the full concentration-gradient oxide after 225 cycles, respectively. On the contrary, the normal $LiNi_{0.6}Co_{0.2}Mn_{0.2}O_2$ oxide suffers from a severe capacity fading, leading to the low capacity of 131.9 mAh g^{-1} and low energy density of 473.6 Wh Kg^{-1} over the same cycle period. To further evaluate the cycle stability of the full concentration-gradient oxide, the operating temperature is increased to 55 °C, as shown in Fig. 8(c). Obviously, the same change tendency is still obtained. More specifically, the large capacity of 173.3 mAh g^{-1} and high energy density of 651.4 Wh Kg^{-1} are retained after 200 cycles. While, the normal $LiNi_{0.6}Co_{0.2}Mn_{0.2}O_2$ oxide shows a rapid decrease in capacity and energy density (159.6 mAh g^{-1} and 592.0 Wh Kg^{-1}) after 200 cycles. Therefore, the full concentration-gradient structure is beneficial to the cycle stability in the potential range of 3.0 to 4.4 V at 25 °C and 55 °C. In addition, it is obvious from Fig 8(b), the charge potential increases gradually and the discharged potential decreases continuously during cycling. However, the normal oxide shows much more variation during cycling, especially the change of potential, as compared with the full concentration-gradient oxide. That is, both the discharge capacity and midpoint potential are unavoidably decayed, leading to the decrease of the energy density of the normal oxide. Here, it is more rational to use the energy density to express the performance of oxide, which is integrated with discharge capacity and midpoint potential.[39] The high-rate performance of both oxides in the potential range of 3.0 to 4.4 V at 25 °C is indicated in Fig 8(d). The similar energy density is achieved for both oxides at low current densities, including 20, 50, 100, 200 mA g^{-1}, but the full concentration-gradient oxide displays higher energy density when the current density is increased to 500 and 1000 mA g^{-1}.

Based on previous report,[40] the surface structure of normal $LiNi_{0.6}Co_{0.2}Mn_{0.2}O_2$ oxide suffers from an irreversible transformation, especially at 55 °C. Here, the mixture of spinel and rock salt phases is developed on the surface of the pristine rhombohedral phase due to the highly oxidative environment that triggers the oxygen loss from the surface of the layered oxides. The presence of the ionically insulating rock salt phase may result in sluggish kinetics, thus deteriorating the capacity retention. It means that the cycle stability is highly related to the surface structure of the oxide. In addition, As above mentioned, NiO phase is usually generated on the surface of the Ni-rich oxides, resulting in high interfacial cell impedance and poor high rate capability.[16-18, 41-42] As for the full concentration-gradient oxide, the outer layer could provide excellently stable structure, and the improved cycle life is achieved, especially at 55 °C. Therefore, the stable outer layer can ensure the excellent cycle stability based on energy density for the full concentration-gradient oxide,

as compared with the normal one.

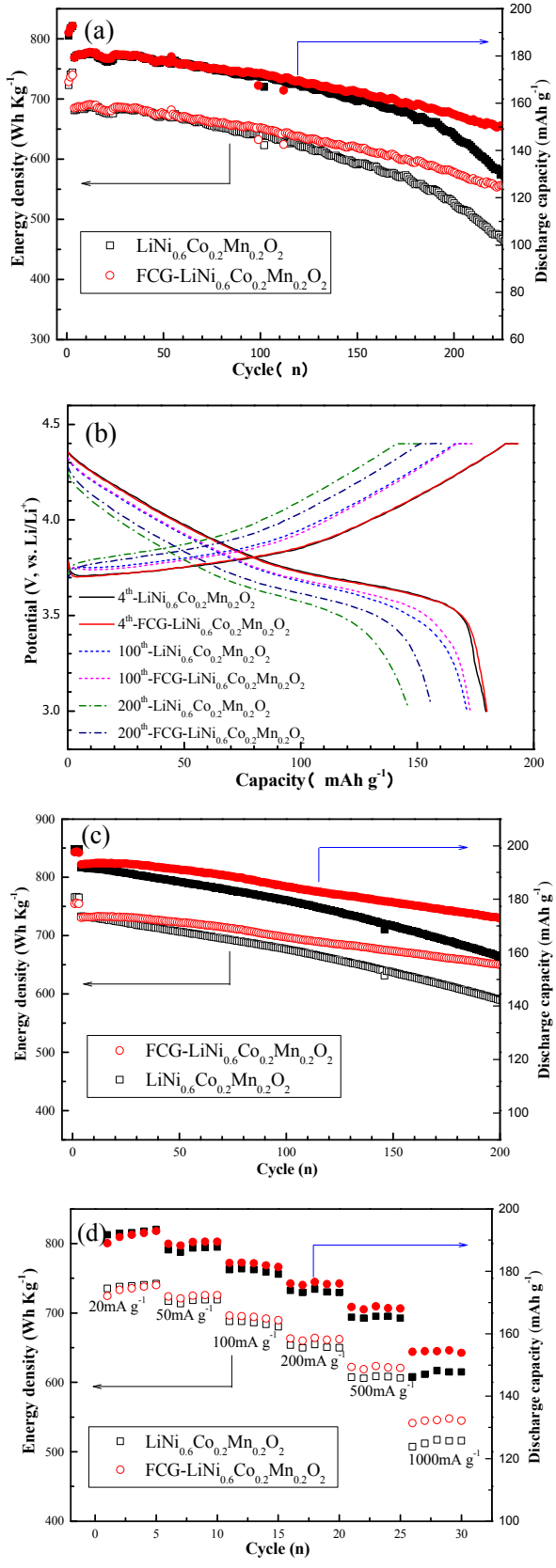

Fig. 8 The Cycle performance at (a) 25 °C and (c) 55 °C, (b) 4th, 100th, 200th charge-discharge curves at 25 °C, and (d) rate property at 25 °C of full concentration-gradient and normal $LiNi_{0.6}Co_{0.2}Mn_{0.2}O_2$ oxides. The energy density is calculated based on the discharge capacity and midpoint potential.

The thermal stability of cathodes plays a great important role in cell safety, especially for the large cells in PHEVs and EVs. Fig. 9 shows the DSC profiles of the full concentration-gradient, and normal $Li_{1-\delta}Ni_{0.6}Co_{0.2}Mn_{0.2}O_2$ electrodes, when charged to 4.4 V at a constant current density of 20 mA g^{-1}. Each electrode shows different tendencies for heat generation. A large exothermic peak in normal $Li_{1-\delta}Ni_{0.6}Co_{0.2}Mn_{0.2}O_2$ electrode appears at 266.2 °C with heat generation of 969 J g^{-1}. On the contrary, the full concentration-gradient electrode exhibits a large exothermic peak at 282.7 °C and low heat generation (692 J g^{-1}). The improved thermal stability of the full concentration-gradient electrode is caused by the thermally stable outer layer, which possess more excellent safety at the highly delithiated state in contrast with normal electrode. Besides, the gradual and continuous concentration change of tetravalent Mn in the out layer gives rise to this enhanced thermal stability, as well as the lithium intercalation stability.[43]

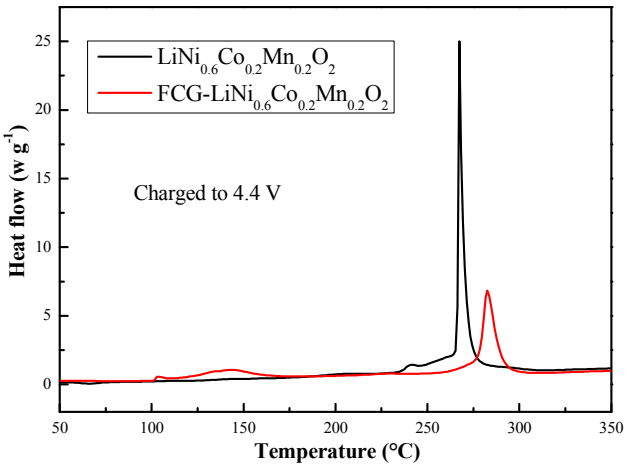

Fig. 9 DSC profiles of full concentration-gradient and normal $Li_{1-\delta}Ni_{0.6}Co_{0.2}Mn_{0.2}O_2$ after initially charged to 4.4 V.

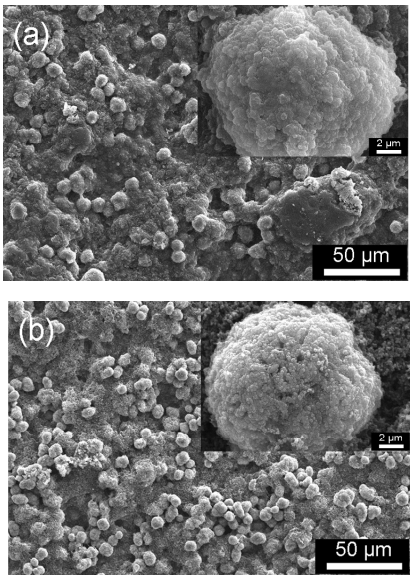

Fig. 10 SEM images of (a) full concentration-gradient and (b) normal $LiNi_{0.6}Co_{0.2}Mn_{0.2}O_2$ electrodes after 200 cycles at 55 °C.

The spherical or ellipsoidal morphologies are still maintained after 200 cycles for both oxides as seen in in Fig. 10. However, the surface of a single particle (inserts) changes much in contrast with original surface as displayed in Fig 6. In particular, the interspace within primary particles of original oxides shrinks due to the volume expansion and pulverization during long cycles.

Fig. 11 (a) shows XRD patterns of the full concentration-gradient and normal $LiNi_{0.6}Co_{0.2}Mn_{0.2}O_2$ electrodes after 200 cycles. The single phase of the layered structure with an $R\bar{3}m$ is maintained after long cycling for both electrodes and impurities are not detected in XRD patterns. The lattice parameters are calculated from XRD patterns, as shown in Table 2. The lattice parameters for the full concentration-gradient oxide are almost identical to those of the original oxide prior to cycling, while the lattice parameters are slightly decreased for the normal $LiNi_{0.6}Co_{0.2}Mn_{0.2}O_2$. It means that the full concentration-gradient oxide presents good structure stability during cycling.

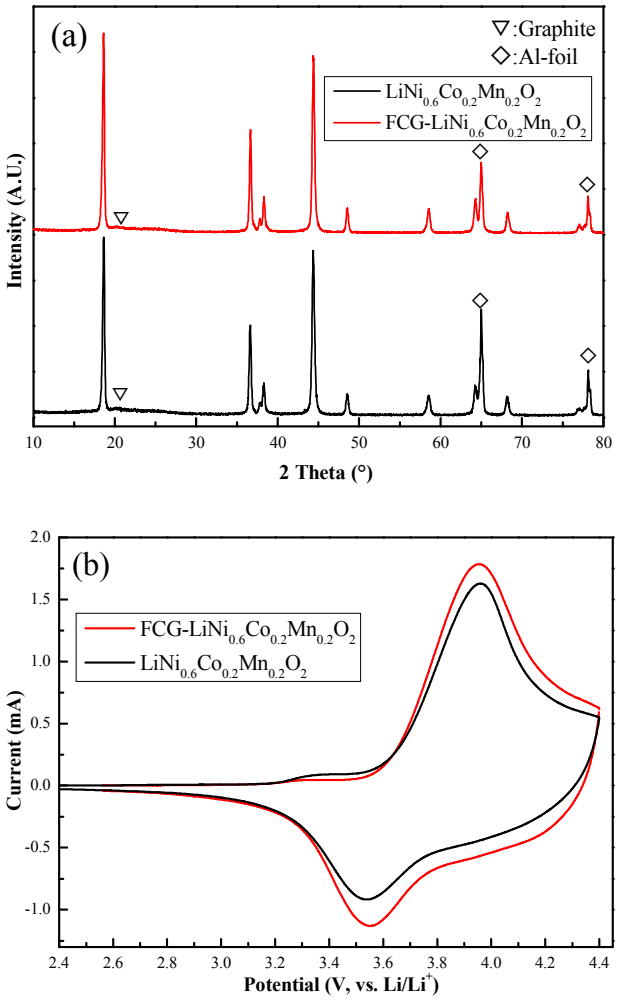

Fig. 11 (a) XRD patterns and (b) cyclic voltammograms of full concentration-gradient and normal $LiNi_{0.6}Co_{0.2}Mn_{0.2}O_2$ electrodes after 200 cycles at 55 °C.

Cyclic voltammograms (CVs) of both electrodes after 200 cycles at 55 °C are shown in Fig. 11(b), in which only one redox couple is obtained, suggesting that structural transitions from hexagonal to monoclinic structure do not occur in the potential range of 3 and 4.4 V, in particular the $Mn^{3+/4+}$ redox reaction peak in the 3 V region.[44] The weak oxidation peak at 4.15 V in Fig. 7(b) disappears for the full concentration-gradient electrode, due to the migration of inner Ni cation to Li sites or out layer during long cycling.[45-46] In addition, the sharp oxidation peak appears at higher potential (about 3.95 V) for both electrodes as compared fresh electrodes with 3.84 V in Fig 7(a), showing the large potential polarization after long cycling. It is more sensitive to use CVs to monitoring the microstructure change of the oxide during cycling.

Table 2 Comparison of lattice parameters of the extensively cycled full concentration-gradient and normal $LiNi_{0.6}Co_{0.2}Mn_{0.2}O_2$ electrodes

	a/Å	c/Å	Vol/Å
Full concentration-gradient material	2.8582	14.1896	100.39
Normal material	2.8517	14.1892	99.93

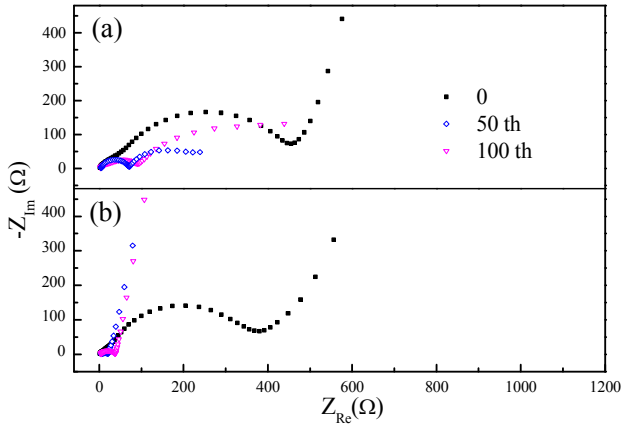

Fig. 12 Impedance spectra of the (a) normal and (b) full concentration-gradient $LiNi_{0.6}Co_{0.2}Mn_{0.2}O_2$ electrodes.

To further understand the origination of the improved electrochemical performance for the full concentration-gradient oxide, electrochemical impedance spectra (EIS) are measured before and after the different charge-discharge cycles at 55 °C. The corresponding Nyquist plots and equivalent circuit model are shown in Fig. 12 and Fig. S1. The plots of the both samples before charging consist of two semicircles in the high-frequency mid-frequency regions and a sloped straight line in the low-frequency region. The semicircles in the high-frequency and mid-frequency regions are related to the surface film resistance and charge-transfer process, respectively. The straight line and arc-like profile in the low-frequency region are attributed to a semi-infinite Warburg diffusion process in the bulk and a finite Nernst diffusion process in a thin layer, respectively.[47] Based on the above analysis, the simulated electrochemical parameters are shown Table S1 by using the equivalent circuit in Fig. S1, in which R_{sf} and R_{ct} mean the surface film resistance and charge-transfer resistance, respectively. W_s and W_o points to the finite Nernst diffusion impedance in the thin layer and semi-infinite Warburg diffusion impedance in the bulk, respectively. Actually, the R_{sf}, R_{ct} and W_o are almost identical for both electrodes before cycle. Differently, after 50 and 100 cycles, the surface film resistance and charge-transfer resistance of the full concentration-gradient sample are much smaller as compared with the normal one. In addition, the normal sample reveals large finite Nernst diffusion impedance in the thin layer, whereas both samples have small semi-infinite Warburg diffusion impedance in the bulk.

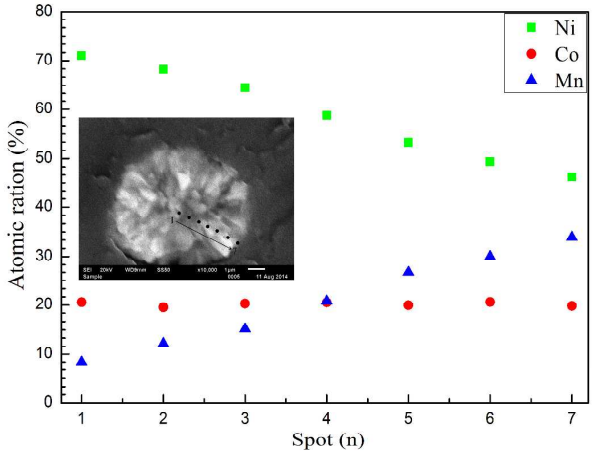

Fig. 13 EDS compositional change from the cross-section of a single full concentration-gradient oxide particle after 200 cycles at 55 °C.

The concentration of Ni, Co and Mn elements in electrolyte after different cycles at 55 °C is provided in Table 3. After 50 cycles, the dissolution of Ni, Co and Mn elements in electrolyte is much lower, where the good cycle performance are observed simultaneously for both electrodes (Fig. 8(c)). However, after 100 and 150 cycles, a large amount of Ni element in electrolyte is detected for the normal oxide, while the dissolution of Ni element in electrolyte is lower for the full concentration-gradient oxide. In addition, it is demonstrated that the full concentration-gradient composition still remains with slightly decreasing the Ni content after 200 cycles at 55 °C (Fig. 13), in consistent with the low dissolution of constituent elements in electrolyte, as well as the high surface reaction activity and fast diffusion kinetics as shown in impedance spectra. Therefore, the full concentration-gradient structure with low Ni content on the surface layer is beneficial to restrict Ni dissolution and ensure good cycle stability during long cycling.

Table 3 The concentration of Ni, Co and Mn elements in electrolyte after different cycles at 55 °C.

	Ni (mg/g)	Co (mg/g)	Mn (mg/g)
Full concentration-gradient oxide			
After 50 cycles	0.22	0.11	0.11
After 100 cycles	1.25	0.25	0.25
After 150 cycles	2.13	0.48	0.47
Normal oxide			
After 50 cycles	0.32	0.19	0.31
After 100 cycles	4.40	0.69	0.46
After 150 cycles	7.14	1.07	0.71

The unique structure with the concentration-gradient composition and spherical morphology is highly important for ensuring good electrochemical performance of the oxide, which is inherited from the hydroxide precursor. Firstly, the micro-nano spherical hydroxide precursor is self-assembled based on the coalescence and Ostwald-ripening mechanisms, in which small particles consume gradually in favor of larger particles to minimize surface free energy via dissolution-recrystallization. The spherical growth of the transition metal hydroxides is usually based on such mechanism, including $Ni(OH)_2$ and $Ni_{1/3}Mn_{1/3}Co_{1/3}(OH)_2$ microspheres.[48-49] Secondly, the formation of the concentration-gradient composition of the hydroxide precursor relies on the transition metal concentration gradient in solution in the co-precipitation process,[50] which can be tailored by the feed time and rate from Mn-rich solution (Tank 1) and Ni-rich solution (Tank 2). Undoubtedly, the formation of the concentration-gradient hydroxide precursor is prerequisite for obtaining the full concentration-gradient oxide with low Ni content on the surface layer, because the transition metal composition is hardly changed in the subsequent calcination process. It is noted that the interfacial reaction is crucial to the cathode performance, including the cycle life and thermal stability.[51-52] As expected, the stable structure with low Ni content on the surface layer is beneficial for improving the thermal stability, decreasing the dissolution of constituent elements in electrolyte, and ensuring good cycle stability of the full concentration-gradient oxide, which are further confirmed by impedance spectra and EDS analysis. Meanwhile, the initial discharge capacity and high rate capability of the full concentration-gradient oxide are comparable to that of the normal oxide. It means that the stable interfacial structure is dominant to stabilize the electrochemical performance of the full concentration-gradient oxide.

Conclusions

In summary, a full concentration-gradient Ni-rich precursors are successfully synthetized via a developed co-precipitation route by well controlling preparation conditions. After lithiation at 800 °C, a Ni-rich lithium transition-metal oxide with the full concentration-gradient structure is achieved, where the Ni concentration decreases linearly, the manganese concentration increases gradually, and cobalt concentration remains constant from the center to surface of each particle based on the EDS results on cross-section of a single particle. As expected, the full concentration gradient oxide presents excellent electrochemical performance, including discharge capacity, cycle stability, high-rate capability and thermal stability. It is believed that the stable outer layer in the full concentration-gradient oxide is beneficial to restrict Ni dissolution, stabilize surface charge-transfer resistance and ensure good cycle stability during long cycling. Therefore, a wide range of functional cathode materials with high energy density can be designed and achieved based on the concept of the full concentration-gradient structure.

Acknowledgements

This work is supported by the National 863 Program of China (2013AA050906), NSFC (51272108), Research Fund for the Doctoral Program of Higher Education (20120031130002) and MOE Innovation Team (IRT13022) of China.

Notes and references

[a] *Institute of New Energy Material Chemistry, Collaborative Innovation Center of Chemical Science and Engineering (Tianjin), Tianjin Key Laboratory of Metal and Molecule Based Material Chemistry, Nankai University, Tianjin 300071, China. Fax: +86-22-23500876; Tel: +86-22-23500876; E-mail: xpgao@nankai.edu.cn*
[b] *School of Materials Science and Engineering, Tianjin University of Technology, Tianjin 300384, China. Fax: +86-22-60214028; Tel.: +86-22- 60214578; E-mail: zhanglianqi@gmail.com*

1 A. M. Andersson, D. P. Abraham, R. Haasch, S. MacLaren, J. Liu, and K. Amine, *J. Electrochem. Soc.*, 2002, **149**, A1358.

2 M. G. S. R.Thomas, W. I. F. David, J. B. Goodenough, and P. Groves, *Mater. Res. Bull.*, 1985, **20**, 1137.
3 M. Broussely, F. Perton, P. Biensan, J. M. Bodet, A. Lecerf, C. Delmas, A. Rougier, and J. P. Peres, *J. Power Sources*, 1995, **54**, 109.
4 I. Saadoune, and C. Delmas, *J. Mater. Chem.*, 1996, **6**, 193.
5 C. Delmas, G. Prado, A. Rougier, E. Suard, and L. Fournes, *Solid State Ionics*, 2000, **135**, 71.
6 H. J. Noh, S. Youn, C. S. Yoon, and Y. K. Sun, *J. Power Sources*, 2013, **233**, 121.
7 X. H. Xiong, Z. X. Wang, H. J. Guo, Q. Zhang, and X. H. Li, *J. Mater. Chem. A*, 2013, **1**, 1284.
8 M. H. Kim, H. S. Shin, D. Shin, and Y. K. Sun, *J. Power Sources*, 2006, **159**, 1328.
9 K. K. Lee, W. S. Yoon, K. B. Kim, K. Y. Lee, and S. T. Hong, *J. Power Sources*, 2001, **97-98**, 308.
10 H. Cao, Y. Zhang, J. Zhang, and B. J. Xia, *Solid State Ionics*, 2005, **176**, 1207.
11 P. Y. Liao, J. G. Duh, and S. R. Sheen, *J. Power Sources*, 2005, **143**, 212.
12 P. Yue, Z. X. Wang , X. H Li, X. H. Xiong, J. X. Wang, X.W. Wu, and H. J. Guo, *Electrochim. Acta*, 2013, **95**, 112.
13 H. Arai, S. Okada, Y. Sakurai, and J. Yamaki, *Solid State Ionics*, 1998, **109**, 295.
14 D. P. Abraham, R. D. Twesten, M. Balasubramanian, I. Petrov, J. McBreen, and K. Amine, *Electrochem. Commun.*, 2002, **4**, 620.
15 S. U. Woo, C. S. Yoon, K. Amine, I. Belharouak, and Y. K. Sun, *J. Electrochem. Soc.*, 2007, **154**, A1005.
16 J. Shim, R. Kostecki, T. Richardson, X. Song, and K. A. Striebel, *J. Power Sources*, 2002, **112**, 222.
17 R. B. Wright, J. P. Christophersen, C. G. Motloch, J. R. Belt, C. D. Ho, V. S. Battaglia, J. A. Barnes, T. Q. Duong, and R. A. Sutula, *J. Power Sources*, 2003, **112**, 865.
18 I. Belharouak, W. Lu, D. Vissers, and K. Amine, *Electrochem. Commun.*, 2006, **8**, 329.
19 C. L. Gan, X. H. Hu, H. Zhan, and Y. H Zhou, *Solid State Ionics*, 2005, **176**, 687.
20 Y. Zhang, H. Cao, J. Zhang, and B. J. Xia, *Solid State Ionics*, 2006, **177**, 3303.
21 P. Y. Hou, J. Guo, D. W. Song, J. Zhang, E. L. Zhou, and L. Q. Zhang, *Chem. Lett.*, 2012, **41**, 1712.
22 X. K. Yang, D. Wang, R. Z. Yu, Y. S. Bai, H. B. Shu, L. Ge, H. P. Guo, Q. L. Wei, L. Liu, and X. Y. Wang, *J. Mater. Chem. A,* 2014, **2**, 3899.
23 Y. K. Sun, S. T. Myung, B. C. Park, J. Prakash, I. Belharouak, and K. Amine, *Natuer Mater.*, 2009, **8**, 320.
24 W. Lu, I. Belharouak, D. Vissers, and K. Amine, *J. Electrochem. Soc.*, 2006, **153**, A2147.
25 S. T. Myung, S. Komaba, K. Hosoya, Y. Miura, N. Hirosaki, and N. Kumagai, *Chem. Mater.*, 2005, **17**, 2427.
26 S. T. Myung, and Y. K. Sun, *Electrochim. Acta*, 2005, **50**, 4800.
27 T. Ohzuku, and Y. Makimura, *Chem. Lett.*, 2001, **8**, 744.
28 S. M. Park, T. H. Cho, and M. Yoshio, *Chem. Lett.*, 2004, **33**, 6.
29 M. H. Lee, Y. J. Kang, S. T. Myung, and Y. K. Sun, *Electrochim. Acta*, 2004, **50**, 939.
30 S. W. Oh, S. H. Park, C. W. Park, and Y. K. Sun, *Solid State Ionics*, 2004, **171**, 167.
31 W. S. Yoon, Y. Paik, X. Q. Yang, M. Balasubramanian, J. McBreen, and C. P. Grey, *Electrochem. Solid State Lett.*, 2002, **5**, A263.
32 G. Cherkashinin, D. Ensling, and W. Jaegermann, *J. Mater. Chem. A,* 2014, **2**, 3571.
33 X. Q. Yang, J. McBreen, W. S. Yoon, and C. P. Grey, *Electrochem. Commun.*, 2002, **4**, 649.
34 Z. Lu, L. Y. Beaulieu, R. A.Donaberger, C. L.Thomas, and J. R. Dahn, *J. Electrochem. Soc.*, 2002, **149**, A778.
35 Y. K. Sun, Z. H. Chen, H. J. Noh, D. J. Lee, H. G. Jung, Y. Ren, S. Wang, C. S. Yoon, S. T. Myung, and K. Amine, *Natuer Mater.*, 2012, **11,** 942.
36 Y. S. Meng, G. Ceder, C. P. Grey, W. S. Yoon, and S. H. Yang, *Electrochem. Solid-State Lett.,* 2004, **7**, A155
37 C. J. Han, J. H. Yoon, W. Cho, and H. Jang, *J. Power Sources*, 2004, **136**, 132.
38 Y. Chen, G. X. Wang, K. Konstantinov, H. K. Liu, and S. X. Dou, *J. Power Sources*, 2003, **119–121**, 184.
39 H. Z. Zhang, Q. Q. Qiao, G. R. Li, and X. P. Gao, *J. Mater. Chem. A,* 2014, **2**, 7454.
40 S. K. Jung, H. Gwon, J. Hong, K. Y. Park, D. H. Seo, H. Kim, J. Hyun, W. Yang, and K. Kang, *Adv. Energy Mater.,* 2014, **4**, 1300787.
41 T. E. Ashton, J. V. Laveda, D. A. MacLaren, P. J. Baker, A. Porch, M. O. Jones, and S. A. Corr, *J. Mater. Chem. A,* 2014, **2**, 6238.
42 X. Q. Yu, Y. C. Lyu, L. Gu, H. M. Wu , S. M. Bak, Y. N. Zhou, K. Amine, S. N. Ehrlich, H. Li, K. W. Nam, and X. Q. Yang, *Adv. Energy Mater.,* 2014, 4, 1300950.
43 Y. K. Sun, H. J. Noh, and C. S. Yoon, *J. Electrochem. Soc.*, 2012, **159,** A1.
44 J. M. Paulsen, C. L. Thomas, and J. R. Dahn, *J. Electrochem. Soc.*, 2000, **147**, A861.
45 M. Gu, A. Genc, I. Belharouak, D. P Wang, K. Amine, S Thevuthasan, D. R. Baer, J. G. Zhang, N. D. Browning, J. Liu, and C. M. Wang, *Chem. Mater.*, 2013, **25**, 2319.
46 H. J. Yu, Y. M. Qian, M. Otani, D. M. Tang, S. H. Guo,Y. B. Zhu, and H. S. Zhou, *Energy Environ. Sci.,* 2014, **7**, 1068.
47 F. Kuang, D. Zhang, Y. J. Li, Y. Wan and B. R. Hou, *J. Solid State Electrochem.,* 2009, **13**, 385.
48 C. Z. Yuan, X. G. Zhang, L. H. Su, B. Gao, and L. F. Shen, *J. Mater. Chem*., 2009, **19**, 5772.
49 A. V. Bommel, and J. R. Dahn, *Chem. Mater*. 2009, **21**, 1500.
50 G. M. Koenig, I. Belharouak, H. X. Deng, Y. K. Sun, and K. Amine, *Chem. Mater*. 2011, **23**, 1954.
51 Q. L. Wei, X. Y. Wang, X. K. Yang, B. W. Ju, B. N. Hu, H. B. Shu, W. C. Wen, M. Zhou, Y. F. Song, and H. Wu, *J. Mater. Chem. A,* 2013, **1**, 4010.
52 Q. Q. Qiao, H. Z. Zhang, G. R. Li, S. H. Ye, C. W. Wang, and X. P. Gao, *J. Mater. Chem. A,* 2013, **1**, 5262.

High-energy, full concentration-gradient cathode material for excellent cycle and thermal stability for lithium ion batteries

P. Y. Hou, L. Q. Zhang, X. P. Gao

TOC

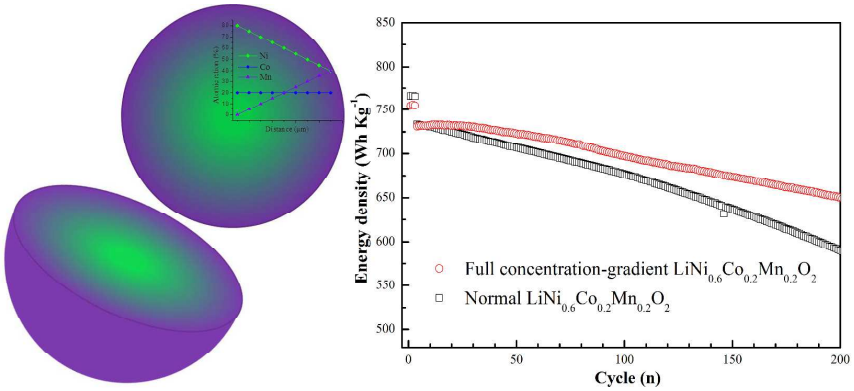

The full concentration-gradient layered oxide presents excellent cycle stability and thermal stability as compared with the normal oxide due to the stable structure with low Ni content on the surface layer.